

GA-A25200

**EDGE STABILITY ANALYSIS
AND PEDESTAL AND ELM CHARACTERISTICS
IN DIII-D DISCHARGES WITH ELM
SUPPRESSION THROUGH EXTERNALLY
APPLIED MAGNETIC FIELD PERTURBATIONS**

by

**T.H. OSBORNE, P.B. SNYDER, T.E. EVANS, R.A. MOYER, M.J. SCHAFFER,
J.A. BOEDO, K.H. BURRELL, R.J. GROEBNER, A.W. LEONARD, D.M. THOMAS,
G. WANG, and L. ZENG**

SEPTEMBER 2005



DISCLAIMER

This report was prepared as an account of work sponsored by an agency of the United States Government. Neither the United States Government nor any agency thereof, nor any of their employees, makes any warranty, express or implied, or assumes any legal liability or responsibility for the accuracy, completeness, or usefulness of any information, apparatus, product, or process disclosed, or represents that its use would not infringe privately owned rights. Reference herein to any specific commercial product, process, or service by trade name, trademark, manufacturer, or otherwise, does not necessarily constitute or imply its endorsement, recommendation, or favoring by the United States Government or any agency thereof. The views and opinions of authors expressed herein do not necessarily state or reflect those of the United States Government or any agency thereof.

EDGE STABILITY ANALYSIS AND PEDESTAL AND ELM CHARACTERISTICS IN DIII-D DISCHARGES WITH ELM SUPPRESSION THROUGH EXTERNALLY APPLIED MAGNETIC FIELD PERTURBATIONS

by

T.H. OSBORNE, P.B. SNYDER, T.E. EVANS, R.A. MOYER,* M.J. SCHAFFER,
J.A. BOEDO,* K.H. BURRELL, R.J. GROEBNER, A.W. LEONARD, D.M. THOMAS,
G. WANG,[†] and L. ZENG[†]

This is a preprint of a paper to be presented at the 10th IAEA
Technical Meeting on H-Mode Physics and Transport Barriers,
September 28-30, 2005, in St. Petersburg, Russia, and to be
published in the *Plasma Phys. & Control. Fusion*.

*University of California-San Diego, La Jolla, California.

[†]University of California-Los Angeles, Los Angeles, California.

Work supported by
the U.S. Department of Energy
under DE-FC02-01ER54698, DE-FG02-04ER54758,
and DE-FG03-01ER54615

GENERAL ATOMICS PROJECT 30200
SEPTEMBER 2005



ABSTRACT

An internal coil system, the I-coil, configured to produce an $n=3$ magnetic perturbation, was used to suppress Type I edge localized modes (ELMs) on DIII-D without significantly reducing core energy confinement, and without a build up of impurities or density. At high collisionality, $\nu_e^* \sim 1$, the I-Coil was effective in suppression of Type I ELMs even when configured with a poloidal variation which is expected to give a relatively low resonance with the equilibrium magnetic field and hence weak stochastization of the edge magnetic surfaces. At $\nu_e^* \sim 1$, the pedestal and core pressure profiles were essentially unchanged between the ELMing and I-coil ELM suppressed phases. When Type I ELMs infrequently occurred in the I-coil phase at $\nu_e^* \sim 1$, their characteristics were similar to ELMs with the I-Coil off, while small, possibly Type II, ELMs, associated with intermittent transport to the vessel walls, became larger and more frequent with the I-coil on. At low collisionality, $\nu_e^* \sim 0.1$, Type I ELMs were eliminated only when the I-coil was configured with a poloidal variation which is expected to give the best resonance with the equilibrium field, and hence produce a stronger stochastization of the edge magnetic surfaces. In this case Type II ELMs were not present and no magnetohydrodynamic (MHD) activity associated with the edge was observed, although some enhancement in broadband density fluctuations from the pedestal region occurred [R.A. Moyer, et al., *Phys. Plasmas* **12**, 56119-1 (2005)]. A range of pedestal pressures were produced by varying the I-coil current and plasma heating power in I-coil ELM suppressed discharges at $\nu_e^* \sim 0.1$, principally through changes in the pedestal density. Stability analysis in these cases indicates that the plasma edge was below the intermediate n peeling/ballooning mode limit.

I. INTRODUCTION

The Type I edge localized mode (ELM) remains a significant concern for reactor scale tokamaks. At the collisionality expected at the top of the ITER H-mode pedestal, $\nu_e^* \sim 0.1$, present day tokamaks near ITER shape and q have ELM energy loss, $\Delta W_{\text{ELM}} > 0.15 W_{\text{PED}}$, where W_{PED} is the pedestal energy, the product of the pedestal pressure and the plasma volume. ELMs of this size are expected to rapidly erode the divertor target plates in ITER [1]. The DIII-D I (internal)-coil (figure 1) has been used successfully to produce discharges free of Type I ELMs while maintaining good energy confinement and avoiding runaway density or impurity accumulation [2,3] (figure 2). Neutral beam heating injected in the direction of the plasma current, co-injection, was used in the I-coil ELM suppression experiments.

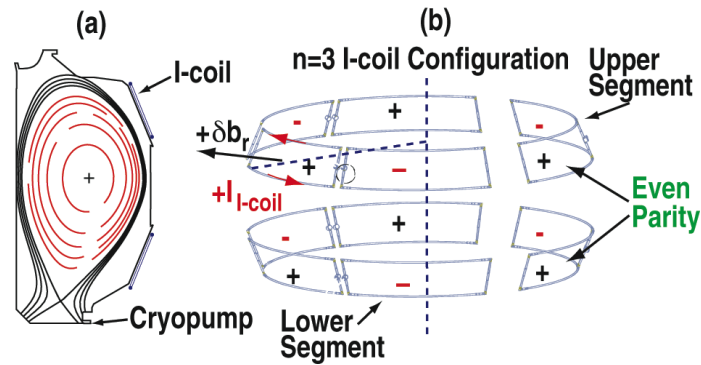


Figure 1. (a) The I-coil is mounted on the inner surface of the outboard wall of the DIII-D vacuum vessel with 12 single turn loops, 6 above and 6 below the midplane. (b) The I-coil was used in an $n = 3$ configuration for the ELM suppression experiments. The upper and adjacent lower loops were configured either with the same sign currents as shown, even parity, or with opposite sign currents, odd parity. The pattern of currents could also be rotated toroidally by one loop or 60 degrees.

The I-coil is composed of 12 single turn loops attached to the inner surface of the DIII-D vacuum vessel with two sets of 6 coils above and below the vessel midplane (figure 1). For these experiments, adjacent coils in a given above or below midplane set were connected to have equal and opposite currents. This produces a magnetic field perturbation with toroidal mode number, n , of 3. This configuration was chosen to avoid lower n components which are less localized to the plasma edge, due to their weaker radial fall off, and which might induce core magnetohydrodynamic (MHD) modes, for example by providing seed islands for neoclassical tearing modes. A current of 3 kA in the I-coil was sufficient to suppress ELMs in 1.3 MA DIII-D discharges. Magnetic field line tracing, which did not include the plasma response or rotational shielding, indicated that the I-coil should produce magnetic islands and bands of stochastic field in the H-mode pedestal region [2,3]. In addition, field lines

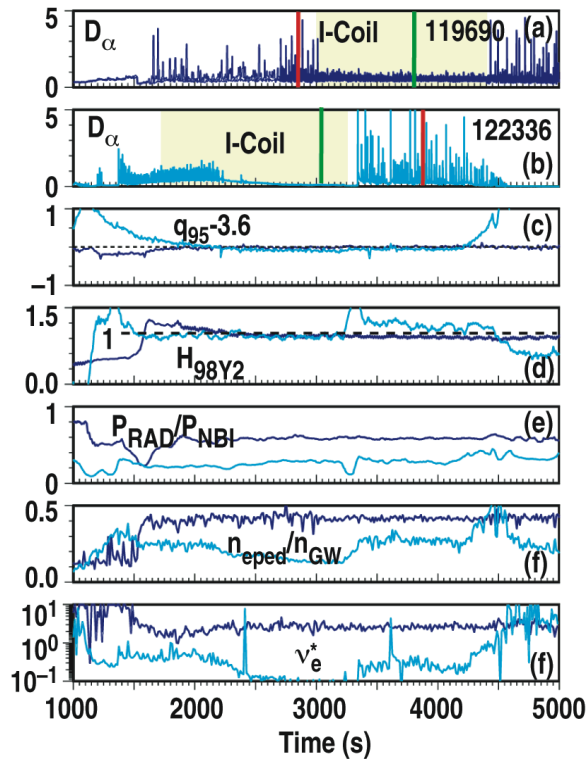


Figure 2. Examples of I-coil ELM suppression for a $v_e^* \sim 1$ discharge with odd I-coil parity shown in dark blue, and a $v_e^* \sim 0.1$ discharge shown in light blue. (a) Divertor D_α signal for a $v_e^* \sim 1$ discharge with the I-coil on period marked in yellow. Analysis times for the green (I-coil on) and red (I-coil off) profiles shown in figure 4 are marked. (b) Divertor D_α signal for $v_e^* \sim 0.1$. Analysis times for the green and red profiles shown in figure 5 are marked. (c) I-coil is most effective in $v_e^* \sim 0.1$ case when q is near the value that maximizes resonance, $q_{95} = 3.6$. (d) H-mode energy confinement enhancement factor stays near 1 (1 = H-mode confinement). (e) Radiated power level is unchanged in the ELM suppressed phase. (f) Pedestal density relative to the Greenwald density. (g) Electron collisionality at the top of the H-mode pedestal.

cross the separatrix and reach the divertor in a narrower region near the separatrix. This break up of the magnetic surfaces was expected to enhance transport in the H-mode pedestal region, possibly maintaining the pressure below the edge stability limit and thus avoiding ELMs, but not destroying the H-mode pedestal and the associated good overall H-mode confinement. The I-coil was connected with either the same signs for coils above and below the midplane, referred to as even parity, or opposite signs across the midplane, referred to as odd parity. To generate large magnetic islands, which overlap producing stochastic field regions, requires that the radial field produced by the I-coil stay in phase with a magnetic field line. This match depends on the pitch of the field near the outboard midplane where the I-coil is located, and on the I-coil parity. Since the local magnetic shear on the outboard midplane is relatively low, if resonance is achieved on one magnetic surface it is typically achieved on many others. For odd I-coil parity a large resonant radial field component is achieved only when the surface averaged q value in the pedestal region is below about 2.5 or above 10. At the more relevant and achievable q of 3.7 the resonant field component is relatively small and the extent of the stochastic field

region is expected to be small (figure 3). For even I-coil parity, the resonant component of the field at $q = 3.7$ is about an order of magnitude larger than in the odd parity case producing significantly larger island overlap (figure 3). Although the resonant component of the I-coil field is an order of magnitude smaller in odd relative to even parity, it should be noted that total radial field perturbation is roughly the same in even and odd parity.

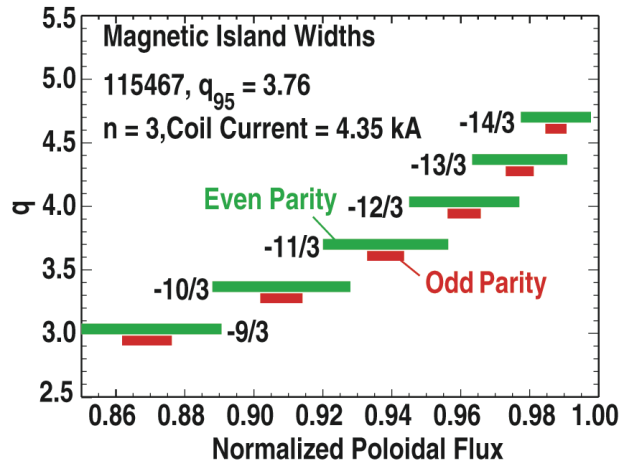


Figure 3. Magnetic island widths computed for a representative equilibrium and typical I-coil current, ignoring any plasma response or rotational shielding of the I-coil field. Even I-coil parity is in green and the odd parity is shown in red. The even parity case has large regions of island overlap that would correspond roughly to the expected regions of stochastic field, while the odd parity case has no island overlap.

In addition to the I-coil, DIII-D has a coil set, the C-coil, that is designed to null out the intrinsic error fields. The C-coil is situated on the midplane and is composed of 6 loops. Interaction between the I-coil and the intrinsic error fields or the C-coil field has an effect on ELM suppression particularly at odd parity where the I-coil resonant field is roughly the same magnitude as the intrinsic error field. This was reflected in the sensitivity of the results to the I-coil toroidal phasing.

The effectiveness of the I-coil in producing stochastic field regions also depends on the plasma cross-sectional shaping. Shaping, for example, affects the spacing of the mode rational surfaces. However the effect of shaping on the extent of the expected stochastic field region is relatively weak. Nevertheless, plasma shape did play a role in the ELM suppression results as described below.

The I-coil effectiveness for ELM suppression as a function of collisionality, I-coil parity, I-coil toroidal phasing, and plasma triangularity, is shown in table 1. Conditions which might be expected to enhance the resonant field perturbation, RMP, effect are 1) even I-coil parity, which increases the RMP amplitude (figure 3), 2) 60 degree toroidal phasing making the I-coil and intrinsic field errors additive, 3) low collisionality giving longer mean free path, allowing particles to move radially

along the stochastic field, 4) low triangularity allowing effective divertor pumping required for reducing the density in H-mode. Although complete ELM suppression was achieved in $v_e^* \sim 1$, odd parity, 0 degree toroidal phasing, and high triangularity, this was unexpected on basis of enhanced transport through edge magnetic field stochastization due to the relatively small resonant field amplitude at odd parity.

Table 1. Effectiveness of ICOIL ELM suppression: (Green) complete suppression, (Yellow) strong reduction in ELM frequency or size, (Red) little change in ELM behavior, (No Color) not tested.

$v_e^* \sim 0.1$, p-even $\phi = 60, \delta < 0.5$	$v_e^* \sim 0.1$, p-even $\phi = 0, \delta < 0.5$	$v_e^* \sim 0.1$, p-even $\phi = 60, \delta > 0.5$	$v_e^* \sim 0.1$, p-even $\phi = 0, \delta > 0.5$
$v_e^* \sim 0.1$, p-odd $\phi = 60, \delta < 0.5$	$v_e^* \sim 0.1$, p-odd $\phi = 0, \delta < 0.5$	$v_e^* \sim 0.1$, p-odd $\phi = 60, \delta > 0.5$	$v_e^* \sim 0.1$, p-odd $\phi = 0, \delta > 0.5$
$v_e^* \sim 1$, p-even $\phi = 60, \delta < 0.5$	$v_e^* \sim 1$, p-even $\phi = 0, \delta < 0.5$	$v_e^* \sim 1$, p-even $\phi = 60, \delta > 0.5$	$v_e^* \sim 1$, p-even $\phi = 0, \delta > 0.5$
$v_e^* \sim 1$, p-odd $\phi = 60, \delta < 0.5$	$v_e^* \sim 1$, p-odd $\phi = 0, \delta < 0.5$	$v_e^* \sim 1$, p-odd $\phi = 60, \delta > 0.5$	$v_e^* \sim 1$, p-odd $\phi = 0, \delta > 0.5$

In section II we discuss the I-coil ELM suppression results at $v_e^* \sim 1$, odd parity, 0 degree toroidal phasing, and high triangularity. In section III the case of $v_e^* \sim 0.1$, even parity, 60 degree toroidal phasing, and low triangularity is discussed. Conclusions and discussion are in section IV.

II. $\nu_e^* \sim 1$, ODD I-COIL PARITY DISCHARGES

Even though the resonant magnetic field perturbation is small in the case of odd I-coil parity, complete Type I ELM suppression was achieved with this configuration in $\nu_e^* \sim 1$, higher triangularity discharges on DIII-D (figure 2). When the ELMs were suppressed the H-mode energy confinement enhancement factor remained unchanged [figure 3(a)], where we use the ITER98y2 scaling [4], $H = \tau_E^{\text{TH}} / \tau_E^{\text{ITER98y2}}$, where τ_E^{TH} is the energy confinement time using the thermal energy content and including a dW/dt correction to the input power, and

$$\tau_E^{\text{ITER98y2}}(\text{s}) = 0.0562 A^{0.19} I_P^{0.93}(\text{MA}) B_T^{0.15}(\text{T}) n_e^{0.41} (10^{19} \text{ m}^{-3}) R^{1.39}(\text{m}) a^{0.58}(\text{m}) \kappa^{0.78} P_{\text{LOSS}}^{-0.67} .$$

The electron density, electron temperature, and ion temperature profiles also changed very little, both overall and in the pedestal region, in the I-coil ELM suppressed phase compared to the ELMing no-I-coil phase of the same discharge (figure 4). There was often a small increase in ion and electron temperatures and decrease in electron density in the pedestal region with the I-coil and Type I ELMs suppressed. There was typically some rise in Z_{eff} across the profile with the I-coil on, where carbon is the only significant contribution to Z_{eff} . The toroidal rotation speed measured for the carbon impurity is typically dramatically reduced with the I-coil on over the entire plasma cross-section, in some cases becoming counter to the neutral beam injection direction in the pedestal region. No cases were observed for which the total pressure profile in the pedestal region in the I-coil ELM suppressed phase was significantly different from the profile before a Type I ELM with the I-coil off under otherwise similar discharge conditions.

In many cases the Type I ELMs are not completely eliminated in the $\nu_e^* \sim 1$, odd parity discharges but continued at reduced frequency. The energy loss associated with the Type I ELMs with the I-coil on, as determined from EFIT reconstruction using fast magnetic probe signals as well as from the change in the total pressure at an ELM from the measured profiles, is found to be roughly the same as for Type I ELMs with the I-coil off. The magnetic fluctuations at a Type I ELM were also similar with the I-coil on and off. As would be expected from the similar pedestal pressure profiles with and without the I-coil, peeling/ballooning mode stability calculations using the ELITE code [5] give similar growth rates and toroidal mode numbers before Type I ELMs with and without the I-coil. Moreover the peeling/ballooning modes are predicted to become unstable at roughly the same fraction of the time between ELMs with and without the I-coil. It should be noted that the edge current density used in all

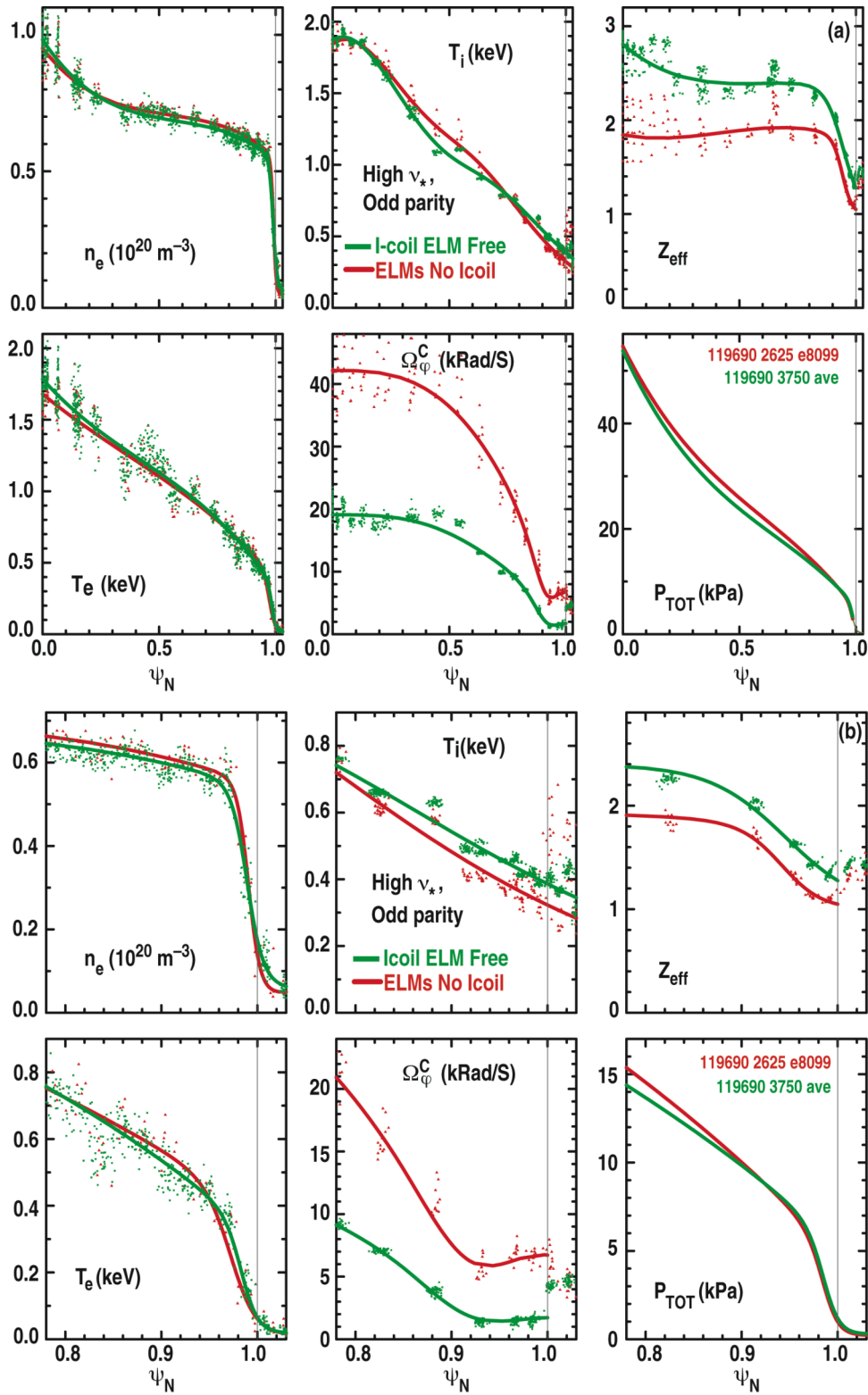


Figure 4. With the exception of a reduction in toroidal rotation speed and some increase in effective charge, profiles in the $v_e \sim 1$, odd I-coil parity discharge shown in figure 3 remain relatively the same with the I-coil on (green curves) or off (red curves), both in the core (a) and in the pedestal region (b). Profiles are plotted with respect to normalized poloidal flux. Profiles of electron density, n_e , electron temperature, T_e , ion temperature, T_i , effective charge assuming carbon as the only impurity, Z_{eff} , toroidal rotation frequency for carbon, Ω_{ϕ}^C , and total pressure P_{TOT} which includes fast ion pressure, are shown.

the stability calculations was taken to be that given by a transport calculation with the edge ohmic current density fully relaxed and with the bootstrap current given by the Sauter model [6]. In discharges without the I-coil this approach to estimating the edge current density has been shown to be in agreement with measurements with the lithium beam system [7], although the validity of this model was not confirmed with lithium beam measurements for discharges with the I-coil on for the stability analysis reported in this paper.

A typical feature of higher density H-mode discharges on DIII-D is the appearance of a series of small ELMs, which are referred to as Type II ELMs, leading up to a larger Type I ELM. These Type II ELMs become larger and fill the time interval between Type I ELMs, while the Type I ELM energy loss decreases, as the density is raised. In contrast to the results on ASDEX-Upgrade [8], the Type II ELMs on DIII-D do not completely replace the Type I ELMs in discharges without the I-coil except at pedestal densities near the Greenwald density where the pedestal pressure is strongly reduced. The Type II ELMs are more edge localized than the Type I as determined from profile reconstruction and soft x-ray observations. The ratio of the midplane to divertor magnetic fluctuation associated with the Type II ELMs is much smaller than for the Type I ELM. For the Type I ELMs the midplane magnetic signals often have a coherent structure which is consistent with the peeling/ballooning mode instability [9].

During the I-coil on phase, in contrast to the Type I ELMs which remain relatively unchanged, the Type II ELMs appear to be enhanced (figure 5), appearing larger on edge soft x-ray signals and in magnetic fluctuations. In some cases with the I-coil on, the Type II ELMs appear in bursts lasting 3-5 milliseconds followed by a quiet period of roughly the same duration. The Type II ELMs themselves are associated with magnetic fluctuations observed on the outboard midplane and in the divertor region with duration of 200-300 microseconds. Although the energy loss associated with individual Type II ELMs was too small to measure with existing techniques, the plasma stored energy before and after one of the Type II bursts was determined using the EFIT reconstruction analysis with fast magnetics. With this technique the loss of plasma stored energy across one of the Type II bursts was roughly 30%-50% of the energy loss in a Type I ELM. The Type II ELMs are also seen on Langmuir probes at the vessel wall and are associated with broadening of the scrape-off layer (SOL) as observed on the reflectometer density profile diagnostic.

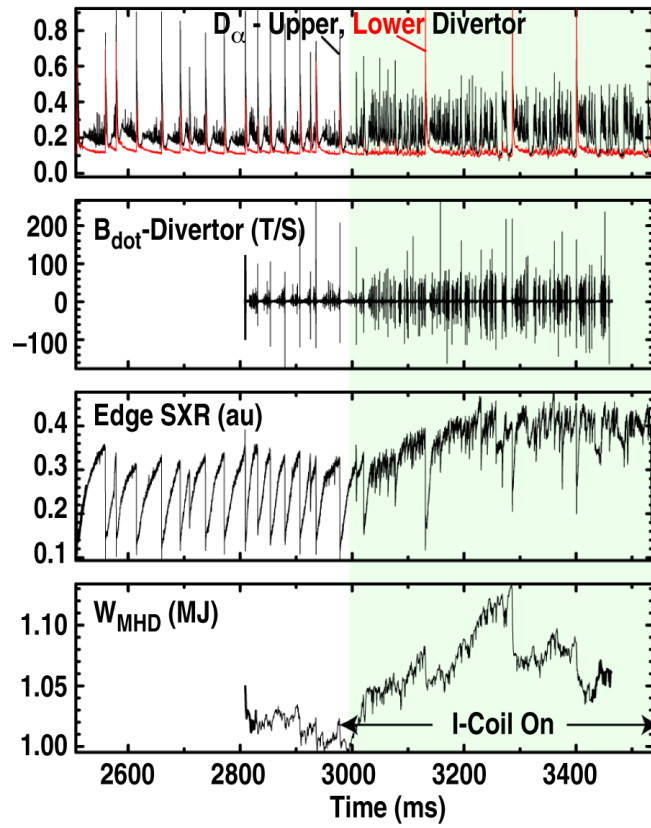


Figure 5. The size of small, Type II, ELMs increase with I-coil on in $\nu_e^* \sim 1$, odd I-coil parity discharge on (a) D_α , (b) magnetic probes in divertor region, and (c) edge SXR. (d) Large Type I ELMs with I-coil on also appear as somewhat larger changes in plasma stored energy compared to I-coil off.

III. $\nu_e^* \sim 0.1$, EVEN I-COIL PARITY DISCHARGES

Complete suppression of Type I ELMs was also achieved at $\nu_e^* \sim 0.1$ and even I-coil parity in lower triangularity discharges. As mentioned in section I, even parity gives the largest resonant field component at $q = 3.6$, and in this case there was a dramatic effect on the profiles including the pedestal region (figure 6). The electron density was strongly reduced with the I-coil on while the electron temperature increased somewhat in the pedestal region but overall remained relatively fixed. The ion temperature increased across the profile possibly due to the decrease in the electron-ion coupling at reduced density. Densities in these discharges even without the I-coil were in the “hot ion” regime where reduced electron-ion coupling and the fact that the neutral beam heating is primarily to the ions can separate the ion and electron temperatures. Z_{eff} increased over the entire plasma cross-section as was also the case at higher collisionality and odd parity. At $\nu_e^* \sim 0.1$ and even I-coil parity, the carbon toroidal rotation velocity decreased in the core but increased in the pedestal region.

The total pedestal pressure was reduced by up to a factor of 2 with the I-coil on compared to the time average pedestal pressure in the ELMing no I-coil phase (figure 6). The magnitude of the edge pedestal reduction increased with increasing I-coil current (figure 7), principally through further reduction in the pedestal density. The H-factor, however, was only reduced by 10%-20%. The fact that the H-factor was not reduced more strongly in response to the pedestal pressure reduction is accounted for by peaking of the density profile ($n_0/n_{\text{PED}} = 3.1$ with the I-coil on and $n_0/n_{\text{PED}} = 1.9$ with the I-coil off in figure 6), by the increase in ion temperature across the profile, and by the increase in fast ion content at reduced density, all of which make the response of the total pressure profile less than proportional to the pedestal pressure as might have been expected for stiff temperature profiles and flat density profiles. In addition the $n^{0.4}$ density dependence in the ITER98y2 confinement time scaling reduces the expectation for the lower density I-coil on phase.

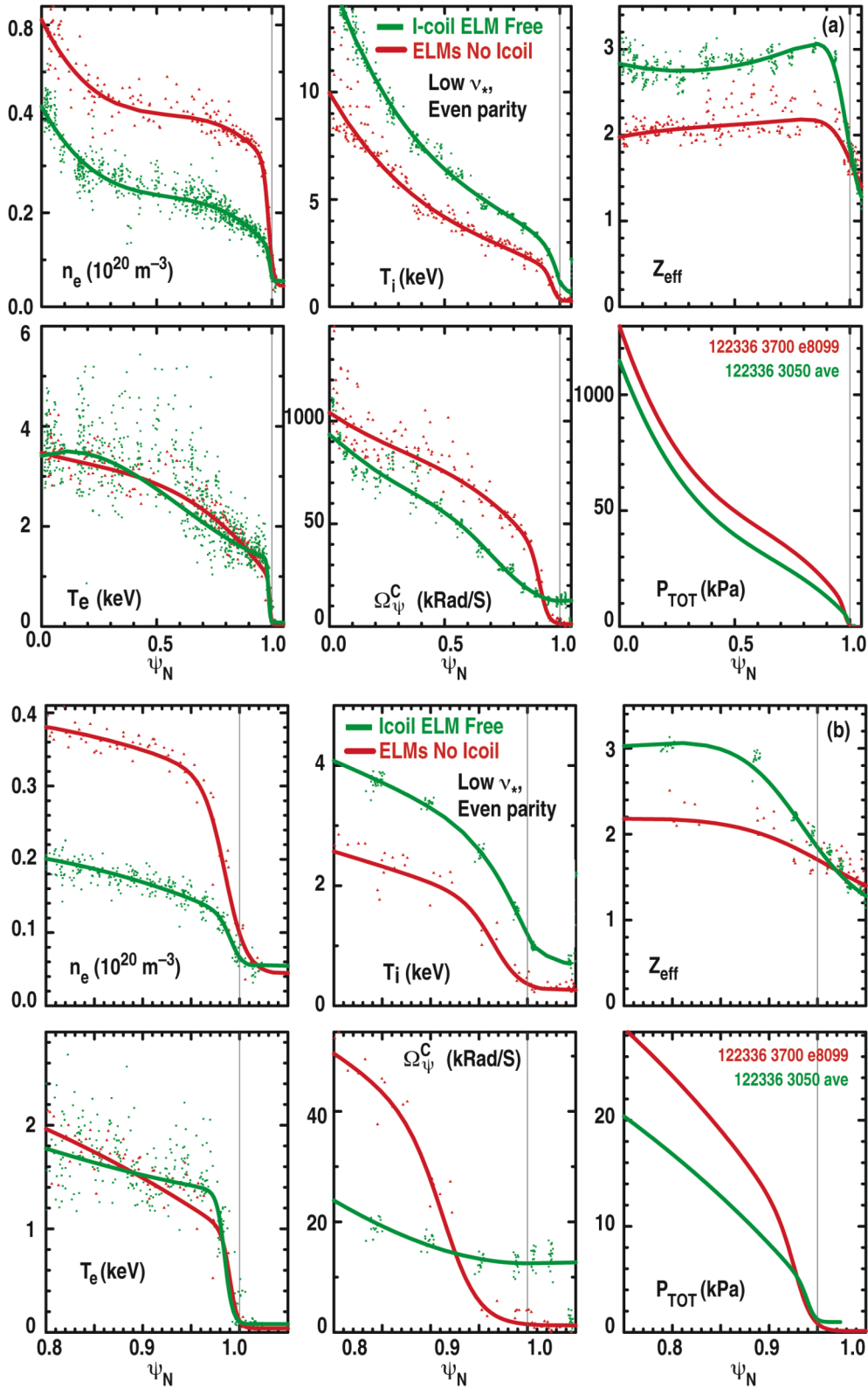


Figure 6. Most profiles show significant change in the $v_e^* \sim 0.1$, even I-coil parity discharge shown in figure 3 between the I-coil on (green curves) and off (red curves) cases, both in the core (a) and in the pedestal region (b). The total pedestal pressure is significantly reduced primarily due to the reduction in pedestal density. The rotation speed is reduced in the core with the I-coil on but increases in the edge consistent with enhanced electron loss. Profiles are plotted with respect to normalized poloidal flux. Individual profiles are as in figure 4.

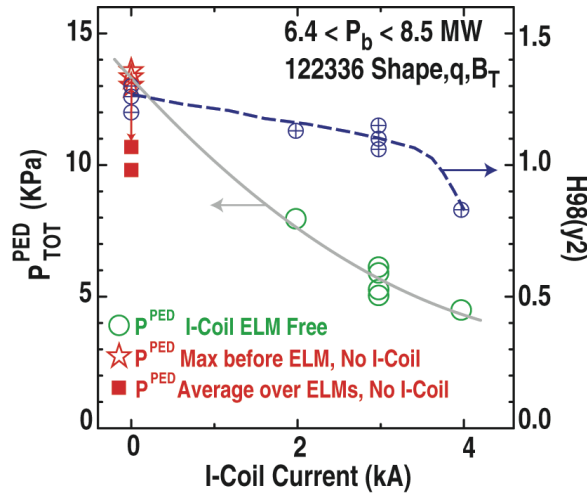


Figure 7. Pedestal pressure is reduced with increasing I-coil current at $\nu_e^* \sim 0.1$, even I-coil parity, comparing pressure just before ELM (red star) to I-coil ELM-free (green circle), the difference is not as great compared to p^{PED} averaged over ELMs (red square); H-factor (blue) is less affected than p^{PED} .

In addition to the reduction in pedestal pressure in the $\nu_e^* \sim 0.1$ and even I-coil parity ELM suppressed discharges, the width of the steep gradient region in the pressure is also reduced. As with the change in pedestal pressure, the width change appears to be the result of changes in the density profile (figure 6), although at the highest I-coil currents there is also some narrowing of the steep gradient region in the electron temperature profile. The edge pressure gradient, however, is reduced with the I-coil on and the discharges are predicted to be stable to peeling/ballooning modes (figure 8).

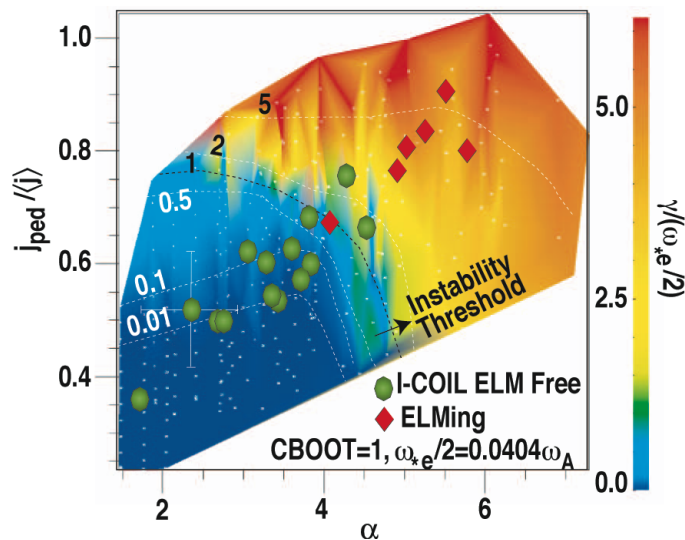


Figure 8. Contour plot of peeling-ballooning mode normalized growth rate versus edge current density and normalized pressure gradient, α , for $\nu_e^* \sim 0.1$, even I-coil parity discharges at fixed cross-sectional shape. I-coil ELM suppressed discharges (green points) are in the stable zone while ELMing discharges (red points) are predicted to be unstable.

No Type II ELMs were observed with or without the I-coil at $\nu_e^* \sim 0.1$. A lack of Type II ELMs is typical of low density DIII-D discharges in general. In contrast to QH-mode [10], which is obtained in a similar density range, no edge harmonic oscillation or other MHD activity associated with the pedestal region was observed in the ELM suppressed discharges. Some increase in broadband density fluctuations was observed in the pedestal region on the beam emission spectroscopy (BES) diagnostic in the ELM suppressed discharges, but there was no evidence for increased intermittent transport to the vessel walls. On the other hand, toroidally and poloidally localized hot spots were observed on the divertor targets with the I-coil on consistent with field lines wandering across the separatrix.

Increasing density with gas puffing in I-coil ELM suppressed discharges raised the pedestal density and pressure and brought back the ELMs. At first the ELMs were small and high frequency but they became larger with increasing gas puffing level. Stability analysis of these discharges indicated that the pedestal became unstable first to higher n , $n \sim 30$, peeling/ballooning modes and then with increasing density and edge pressure to lower n , $n \sim 15$ modes.

IV. DISCUSSION

The ability of a relatively simple external coil set to suppress Type I ELMs while maintaining good energy confinement is a positive result for future tokamaks. At ITER relevant collisionality, $\nu_e^* \sim 0.1$, and even I-coil parity, where the resonant magnetic perturbation should be strong, the pedestal pressure was controlled and maintained below the peeling-ballooning mode stability limit while providing enough particle transport to avoid density or impurity accumulation. Enhancements of the technique could, in principle, allow I-coil ELM-free operation with pedestal pressure above the time averaged value with ELMs. We have estimated that for coils in the $n = 3$ configuration as used in DIII-D, placed on the outside of the vessel wall in ITER, a current of about 140 kA-turns would be required to produce the same level of field perturbation, $B_n/B_T = 3 \times 10^{-4}$, which was sufficient for complete ELM suppression on DIII-D.

The control of pedestal pressure obtained in the low collisionality, even parity discharges may be a direct result of transport produced by the field stochasticization. However, if this were the case it is not obvious why the strongest effect would be on the density profile since parallel transport should strongly affect the temperature. The appearance of hot spots in the divertor with the I-coil suggests a direct effect of the I-coil. However there is some evidence of increased density fluctuations in the pedestal region in the ELM suppressed phase which suggests an instability may be involved.

In the case of ELM suppression at $\nu_e^* \sim 1$, and odd I-coil parity, where the part of the I-Coil field resonant with the equilibrium is small, the evidence suggests an indirect effect through the ELM instability. The Type II ELMs, which appear to be enhanced with the I-coil on, may provide enough transport to avoid reaching the stability limit for the Type I. However, from this point of view, it is difficult to understand the fact that the pedestal pressure profile is quite similar in discharges where the Type I ELMs were completely suppressed compared to the pressure profile just before a Type I ELM with the I-Coil off. No evidence was found which would suggest that the peeling/ballooning mode associated with the Type I ELM was transformed into a continuous instability. No such continuous instability was observed, while very similar rapidly growing MHD activity was seen on the outboard midplane probes before a Type I ELM, and the Type I ELM was associated with about the same energy loss, with the I-Coil on and off. These results suggest that the Type II ELM has a very similar pressure gradient limit to the Type I and therefore is also likely the result of the peeling/ballooning instability but that for some reason the nonlinear phase of the instability is weaker or access to a transport port channel is

reduced compared to the Type I. The Type II ELMs, or the I-Coil directly, might alter a feature other than the pressure profile which is critical for triggering large growth of the peeling/ballooning mode. It is possible there is a difference in the pedestal current density with the I-coil on and off, since this was not directly measured and is known to play a role in the peeling/ballooning stability, for example setting the toroidal mode number [5]. Changes in the rotation speed with the I-Coil on can be ruled out as altering the ELM instability since the Type I ELMs disappear before the rotation changes [3].

References

- [1] G. Federici, et al., J. Nucl. Mater. **313-316**, 11 (2003).
- [2] R.A. Moyer, et al., Phys. Plasmas **12**, 56119-1 (2005).
- [3] T.A. Evans, et al., Phys. Rev. Lett. **92**, 235003-1 (2004).
- [4] ITER Physics Basis Editors, Nucl. Fusion **39**, 2208 (1999).
- [5] P.B. Snyder, et al., Phys. Plasmas **9**, 2037 (2002).
- [6] O. Sauter, et al., Phys. Plasmas **6**, 2834 (1999).
- [7] D.M. Thomas, et al., Phys. Rev. Lett. **93**, 065003 (2004).
- [8] J. Stober, et al., Nucl. Fusion **41**, 1123 (2001).
- [9] C.P. Perez, et al., Nucl. Fusion **44**, 609 (2004).
- [10] K.H. Burrell, et al., Phys. Plasmas **12**, 056121 (2005).

ACKNOWLEDGMENT

This work was supported in part by the U.S. Department of Energy under DE-FC02-04ER54698, DE-FG02-04ER54758, and DE-FG03-01ER54615.